Numerical Study on Ultra-Lean Rotating Counterflow Twin Premixed Flame of Hydrogen-Air

Akane Uemichi and Makihito Nishioka

Department of Engineering Mechanics and Energy, University of Tsukuba

Tsukuba, Ibaraki, 305-8573, Japan

Corresponding Author:

Akane Uemichi

Department of Engineering Mechanics and Energy, University of Tsukuba

1-1-1, Tennodai, Tsukuba, Ibaraki, 305-8573, Japan

Phone: +81-29-853-5944

FAX: +81-29-853-5207

E-mail: akane@uemichi.net

Colloquium: Laminar Flames

s**Numerical Study on Ultra-Lean Rotating Counterflow Twin Premixed Flame of Hydrogen-Air**

Akane Uemichi and Makihito Nishioka
Department of Engineering Mechanics and Energy
University of Tsukuba

ABSTRACT

Rotating counterflow twin premixed flame (RCTF) of hydrogen air was numerically simulated with detailed chemistry to explore the possibility of ultra-lean combustion. As a result, it was found that ultra-lean RCTF of equivalence ratio $\phi = 0.052$, which is far leaner than the generally-recognized flammability limit $\phi = 0.10$, is realized. It was also found that under ultra-lean conditions the flame temperature of RCTF largely exceeds the adiabatic flame temperature; e.g., at $\phi = 0.06$ the former is 1171 K, while the latter is 503 K. This increase of burned gas temperature is attributed to the so-called low Lewis number effect within the flammability limit, but under an ultra-lean condition some other mechanism to increase temperature is dominant. The "pseudo local equivalence ratio" of burned gas of RCTF differs largely from that of the unburned gas due to the extraordinarily high concentration of H_2O. This suggests the possibility that the local condition at the reaction zone is much richer than the unburned gas, which brings about the large temperature increase.

Keywords: Ultra-lean premixed flame, Hydrogen-air flame, Rotating counterflow twin flame, Lewis number effect

INTRODUCTION

Depletion of fossil fuel is one of the most serious problems the whole world is facing, so a high-efficiency utilization of the fuel must be promoted not only by developing novel technologies but also improving existing conventional technologies such as combustion. In the field of combustion, lean-burn technique has been attracting attentions because of its cleanness and high-efficiency [1]. As a representative lean-burn combustion device, swirl combustors have been studied mostly for practical purposes. It is well known that swirl flow has an effect to stabilize very lean premixed flames, but theoretical understanding of the lean-burn mechanism in such practical combustors has not been obtained sufficiently so far, because of the high complexities of turbulent flow and transports.

In the case of a swirl combustor, a large recirculation zone is formed in the burned gas due to the centrifugal force, which is thought to play an important role to stabilize the flame. Therefore, for understanding the lean-burn mechanism in such a combustor, it is essential to elucidate the effect of backflow of burned gas on the flame stability theoretically. For this purpose, recently the authors conducted a detailed-chemistry numerical calculation of methane-air rotating counterflow twin premixed flame (RCTF) [2], which suffers a backflow of burned gas when the rotation rate is sufficiently large. This flame has the originality that the counterflowing burned gas is the one produced by the flame itself, unlike the counterflow flame of premixed gas and independently given burned gas, which has been studied by many researchers. In the study, they found that ultra-lean combustion of the equivalence ratio 0.32 can be realized without radiative heat loss, and that under such an ultra-lean condition the reaction zone is formed in the backflow region. They also found that when the reaction zone is located in the latter region its flame thickness is significantly reduced due to an unusual balance between heat conduction and convection. They suggested the possibility that similar phenomenon may occur locally in practical swirl combustors.

In this study, we applied the same flame model to hydrogen-air case. Hydrogen is now attracting attentions as a CO_2 free fuel from a practical standpoint, while it has long been studied actively from the standpoint of fundamental combustion science, since its flames have various peculiarities caused by its high diffusivity and high exothermicity. For example, the phenomenon of flame ball [3,4], which is observed in very lean hydrogen-air mixture, has been investigated actively as a unique phenomenon governed by a mechanism quite different from that of ordinary premixed flames. The purpose of the present study is to explore the possibility of ultra-lean combustion of hydrogen-air under the existence of backflow of burned gas using RCTF model, and to identify whether a new phenomenon due to the uniqueness of hydrogen occurs or not in such a flame.

NUMERICAL METHOD

Figure 1 shows the theoretical model of RCTF, which is identical with the previous study [2]. RCTF was first experimentally studied by Chen et al. [5]; they investigated the flame behavior in counterflow rotating jets and onset of flow recirculation. From a pair of infinitely large injection planes rotating in the same direction, premixed gases are injected to form a swirling counterflow. Twin flames are formed reflection-symmetrically on the both sides of the stagnation plane. When the rotation rate is not so large the flow and the flames are roughly sketched as Fig. 1(a), but as the rotating rate is increased over some critical value, a backflow region is formed as shown in Fig. 1(b). The governing equations of RCTF are also identical with Ref. 2.

The distance between the two injection planes is 3.0 cm, but because of the symmetricity only the lower half of the domain, i.e., $-1.5 \le x \le 0.0$ cm, is solved. For simplicity, we assumed that the air is composed of 79 % N_2 and 21 % O_2. The unburned gas temperature at the injection plane is set 298 K. The adopted chemical kinetics scheme is a H_2 combustion mechanism obtained by deleting all C-related reactions from the propane combustion mechanism by Qin et al. [6]. The resultant scheme involves 9 species and 28 sets of elementary reactions. RCTF's were solved by using a modified version of PREMIX [7]. For comparison, 1D planar premixed flames were also solved with the original PREMIX. Equilibrium composition and temperature were calculated by using the equilibrium code EQUIL included in the distribution package of CHEMKIN [8].

RESULTS AND DISCUSSION

Extension of the flammable region

First of all, we will show around the edge of the lean-side flammable region of RCTF. Figure 2 shows the response of the maximum temperature T_{max} to the change of the equivalence ratio ϕ. In the top part of Fig. 2 the injection velocity u_R is fixed 400 cm/s with the rotating rate Ω being a parameter, while in the bottom part Ω is fixed 100 rps with u_R a parameter. Dashed lines in both parts show the adiabatic flame temperature T_{eq}. Each response curve has its upper branch and lower branch with a turning point between them, which is the "lean extinction limit" for a set of conditions (Ω, u_R). It is seen that as Ω becomes larger or u_R becomes smaller, the lean extinction limit moves to the lean side. In the figure, the leanest extinction limit is $\phi = 0.052$ for (Ω, u_R) = (100 rps, 400 cm/s); this equivalence ratio is far lower than the generally recognized flammability limit $\phi = 0.10$ of hydrogen-air combustion [9], so this condition can be referred to as an ultra-lean condition. It should be also noted that T_{max}'s in all upper branches in the figure are much higher than T_{eq}, and along each upper branch the deviation is increased with the reduction of ϕ. The deviation amounts to about 670 K at the extinction point for (Ω, u_R) = (150 rps, 400 cm/s). This value is surprisingly larger than 50 K in

the case of methane-air RCTF [2].

Figure 3 shows the maximum flame temperature T_{max} and the burning velocity Su of 1D flame as functions of the equivalence ratio ϕ. Note that the ordinate for Su has a logarithmic scale. We failed to obtain any result for the conditions leaner than $\phi = 0.127$ since the convergence is extremely difficult. Figure 4 compares the flame structure between a 1D flame and a RCTF for $\phi = 0.15$. Other conditions of the RCTF are (Ω, u_R) = (150 rps, 400 cm/s). Note that the horizontal scales are quite different. In the RCTF case, the calculation domain is $-1.5 \le x \le 0.0$ cm and the flame thickness is less than 0.5cm. In contrast, in the 1D flame case, the calculation domain of 100m was needed and the obtained flame thickness is about 50m, which is unrealistically larger than ordinary laboratory scales. It is well known that in the case of hydrogen-air flame near the lean flammability limit a variety of multidimensional instabilities occur experimentally [3,10], so a stable smooth flame comparable to 1D numerical calculation is inherently impossible. Recently, Williams and Grcar [11] performed numerical simulations of "very-lean" hydrogen-air premixed flame. Even in their study, premixed flame in the condition leaner than ϕ = 0.30 is difficult to solve without the "flame ball model." Therefore, it is thought to be meaningless to compare the flame between experiments and 1D numerical calculations in this region.

In Fig. 4, comparing the structures of two flames, much larger concentration of H_2O is observed in the RCTF in addition to the much higher temperature. Deviation of concentration between RCTF and 1D flame was also observed for CO_2 and H_2O in the case of methane-air [2], but their magnitude of differences were much smaller than the present result.

Formation of backflow zone of burned gas

Figure 5 compares the variation of the flame structure of RCTF with Ω, for (ϕ, u_R) = (0.20, 400 cm/s). The top part shows the distributions of the temperature and the heat release rate (HRR), while the bottom shows that of the axial velocity u. In Fig. 5, there is a little bulge in u as a result of gas expansion, which may affect the flame stretch. In the cases of $\Omega = 0$ and $\Omega = 50$rps, the reaction zone defined by HRR is located closely to the plane of symmetry, x = 0.0 cm, which implies that the twin flames are getting close and almost merged. In the case of counterflow twin flame without rotation, it is well known that merging flames must cause incomplete combustion [12]. In the cases of $\Omega = 100$ rps and $\Omega = 150$ rps, on the other hand, the flame surface is located sufficiently far from the plane, i.e., the twin flames exist almost independently. Furthermore, in the high Ω cases, there emerges an additional, secondary stagnation plane in the flame zone, which indicates the formation of backflow caused by a large circumferential force [2]. In the figure, the positions of the secondary stagnation planes, x_{stag}, are shown with vertical lines.

Note that the flames of $\Omega = 0$ and $\Omega = 50$ rps in Fig. 5 are very close to the lean extinction limits that are shown in the top part of Fig. 2. In these cases, the burning velocities do not seem to be so large as to propagate against the convection. Consequently, the reaction zone is pressed on the plane of symmetry by the convection, and further decrease of ϕ will bring about flame extinction due to incomplete combustion. This is the extinction mechanism along the response curves for $\Omega = 0$ and $\Omega = 50$ rps in Fig. 2. In the cases of $\Omega = 100$ rps and $\Omega = 150$ rps, on the other hand, the flame is stabilized far from the plane of symmetry with the help of the backflow, even though its burning velocity is low. It is seen that a region of small axial velocity u spreads around the secondary stagnation point, in which the reaction zone is staying still.

Figure 6 compares the variation of the flame structure with Ω, for (ϕ, u_R) = (0.08, 400 cm/s). Note that these flames are under ultra-lean conditions. As Ω becomes large, the position of secondary stagnation plane, x_{stag}, and the reaction zone move to the upstream. Moreover, the reaction zone is located downstream of the secondary stagnation plane, unlike the $\phi = 0.20$ case in Fig. 5, which means that the flames apparently have negative local burning velocities. Figure 7 shows the local burning velocity Su_L, the location of the secondary stagnation plane x_{stag}, and the reaction zone position x_{Qmax} defined by the maximum heat release, as functions of the equivalence ratio ϕ for the cases of $\Omega = 100$ and 200rps. Here, we defined Su_L as the axial mass flux at x_{Qmax} divided by the unburned gas density. As ϕ is decreased beyond 0.12, the relative position between x_{stag} and x_{Qmax} switches, and Su_L becomes slightly negative. This negative burning velocity must be an only apparent phenomenon, so in reality the flame is thought to have lost its self-propagation nature already, and stand still in a very small convection field being supported by reactants diffusions and heat conduction just as diffusion flames. All these behaviors of ultra-lean RCTF are basically the same as the methane-air case [2].

Lewis number effect

It is well known that hydrogen flames suffer a variety of low Lewis number effects. One representative example is the flame temperature increase of lean hydrogen-air premixed flame under a positive flame stretch, which is explained as an unbalance between the “chemical enthalpy” transport by deficient reactant diffusion and the heat conduction in the preheat zone [13]. Therefore, it is natural to suspect that the extremely large increase of the flame temperature of RCTF in Fig. 2 is caused according to this mechanism. Here, in order to examine the above unbalance in RCTF, the distributions of the chemical enthalpy flux by H_2 diffusion and the conductive heat flux, along with those of temperature and H_2 concentration, are plotted in Fig. 8. The equivalence ratio of (a) and (b) are $\phi = 0.50$ and $\phi = 0.06$, respectively, with other conditions being common, (u_R, Ω) = (400 cm/s,

150 rps). We defined the chemical enthalpy flux as $Q_{H2}\rho Y_{H2}V_{H2}/W_{H2}$, where ρ is the density, and Q_{H2}, Y_{H2}, V_{H2} and W_{H2} are the heat of combustion, mass fraction, axial diffusion velocity and the molecular weight of H_2, respectively. Q_{H2} (J/mol) is defined as the enthalpy change by the overall reaction $H_2 + (1/2)O_2 \Rightarrow H_2O$ at the unburned gas temperature. Chemical enthalpy flux means the flux of "potential heat" accompanied by the diffusion of unburned H_2. Since its unit is the same as the conductive heat flux, quantitative comparison between the two fluxes is possible.

It is seen in Fig. 8(a) that the chemical enthalpy flux largely exceeds the conductive heat flux, which is a natural consequence of the Lewis number less than unity. In this flame, the ratio of the peak absolute value of the chemical enthalpy flux and that of the conductive heat flux is 2.35, and the flame temperature is 1824 K, which is 178 K higher than T_{eq} = 1646 K. Since a RCTF under this condition does not have a back flow region, the flame suffers a positive flame stretch just as an ordinary counterflow twin flame, so the large unbalance of the fluxes brings about the temperature increase from T_{eq} [13]. On the other hand, in the case of the ultra-lean flame of Fig. 8(b), such a large unbalance is not observed. On the contrary, the peak conductive heat flux is somewhat larger than that of the chemical enthalpy flux in spite of the fact that the flame temperature attains 1171 K, which amazingly is 668 K higher than T_{eq} = 503 K. This means that the above-mentioned mechanism of increasing flame temperature cannot be applied to this flame at all. Undoubtedly, there must be some other powerful mechanism of increasing temperature exits in this flame.

Pseudo local equivalence ratio

In addition to the unbalance discussed in the previous section, large difference of diffusivity between H_2 and O_2 brings about variations of local equivalence ratio. This is one aspect of so-called preferential diffusion. In order to evaluate this effect, we introduced the "pseudo local equivalence ratio" by ϕ_{PL} = 0.5[H]/[O], where [X] denotes atom mole fraction of element X. In calculating [X], all species including radicals and final product are taken into account. By adopting this formula, the influence of the above phenomenon can be evaluated even in the flame zone and the burned gas.

Figure 9 compares the distribution of ϕ_{PL} for various ϕ under the condition of (u_R, Ω) = (400 cm/s, 100 rps). In the figure, reaction zone positions, x_{Qmax}, are indicated with short vertical lines. It is seen that for each case ϕ_{PL} starts to decrease as it enters the preheat zone, and then turns to increase to a value larger than the original ϕ. In the preheat zone H_2 is transported towards the reaction zone very fast, while the slower O_2 is left behind, which brings about the former decreases by the reduction of the ratio H_2/O_2. The subsequent increase ϕ_{PL} is thought to be mainly caused by the large concentration of H_2O that will be discussed in the next paragraph. In all cases in the figure, ϕ_{PL}

reaches the maximum value $\phi_{PL,max}$ at the plane of symmetry, and the increase rate of $\phi_{PL,max}$ becomes larger as ϕ is decreased. In the case of ϕ = 0.07 and Ω = 100rps, $\phi_{PL,max}$ amounts to 371 % of the original ϕ in the unburned gas. It must be noted that the reaction zone is located at the shoulder on each curve, which shows that the reactions are proceeding under the condition of ϕ_{PL} close to $\phi_{PL,max}$. Figure 10 shows the ratio of the maximum $\phi_{PL,max}$ and the original ϕ, as a function of ϕ for various rotation rates. As ϕ is decreased the ratio $\phi_{PL,max}/\phi$ becomes larger; around ϕ = 0.05, $\phi_{PL,max}/\phi$ amounts to more than four times larger than the original ϕ.

Here, it should be noted that the concentration of H_2O of the RCTF is much larger than that of the 1D flame as shown in Fig. 4. Since the overall H_2 oxidation reaction is $H_2 + 0.5O_2 \Rightarrow H_2O$ and the H_2 mole fraction in the unburned gas is much smaller than unity, the mole fraction of H_2O in the burned gas should not differ so much from that of H_2 in the unburned gas. In the case of the RCTF in Fig. 4, however, the mole fraction of H_2O is about twice that of H_2. The same phenomenon is also observed in the flames under ultra-lean conditions shown in Fig. 6. This increase of H_2O concentration has the effect of increasing ϕ_{PL}, since ϕ_{PL} of H_2O itself is unity.

Although the large increase of ϕ_{PL} is the mathematical consequence of the high concentration of H_2O, it is expected that the increase would be closely related to the large temperature increase observed in Fig. 2. One possibility is that the ϕ_{PL} at the reaction zone determines the burned gas temperature as the adiabatic flame temperature T_{eq} for the ϕ_{PL}, as well as the composition the gas. Here, in the case of (ϕ, u_R, Ω) = (0.07, 400 cm/s, 100 rps), which is the case of the lowest ϕ in Fig. 9, T_{max} and $\phi_{PL,max}$ are 1184 K and 0.260, respectively, and the adiabatic flame temperature for ϕ = 0.260 is T_{eq} = 1083 K. This disagreement of 101 K between T_{max} and T_{eq} is too large to fully support the above hypothesis, but it remains one candidate mechanism governing the phenomenon. Further study is needed to elucidate the mechanism of increasing the H_2O concentration and the temperature of the burned gas of RCTF.

Effect of radiative heat loss

For simplicity, in the above results radiative heat loss has been excluded. But it is important to check its effect on the flammability limit and the flame structure quantitatively, since it is well known that near the lean flammability limit radiative heat loss plays a key role in the flame extinction [14], and water vapor is known as highly radiative gas. We adopted the optically thin model presented by Barlow et al. [15], with which the additional radiative heat loss term is given as $-4\sigma p(T^4-T_0^4)X_{H2O}a_{p,H2O}$, where p is the pressure, σ is the Stefan-Bortzmann constant, and X_{H2O} and $a_{p,H2O}$ respectively denote the mole fraction and Plank's mean absorption coefficient of the H_2O.

Figure 11 compares the response of the maximum temperature T_{max} of RCTF to the change

of ϕ, in which solid lines and dashed lines show the cases with and without radiative heat loss, respectively. For each u_R, by including the radiative heat loss the leanest extinction limit is shifted to the richer side, although the shift is not so large. In the case of u_R = 200 cm/s, the deviation of the critical ϕ between with and without radiative heat loss is so small as 0.01, and it is much smaller in the case of u_R = 400 cm/s.

Figure 12 compares the flame structure of the RCTF between with and without radiative heat loss for the condition of (ϕ, u_R, Ω) = (0.07, 400 cm/s, 150 rps), which is close to the lean extinction limit. Solid lines and dashed lines show the results with and without radiative heat loss, respectively. It is seen that by considering the radiative heat loss the temperature, the heat release rate, and the concentration of O_2 decrease slightly, while the concentrations of H_2O and H_2 slightly increase. In the methane-air case we found that the radiative heat loss by H_2O, CH_4, CO_2 and CO largely affects the lean extinction limit and flame structure [2]. In the case of H_2-air RCTF, however, the influence of the radiative heat loss only by H_2O is much smaller. In the case of hydrogen-air RCTF, the results obtained without considering radiative heat loss should have sufficient validity.

CONCLUDING REMARKS

By conducting numerical calculations of hydrogen-air rotating counterflow twin premixed flames (RCTF) with detailed chemistry, the following knowledge has been obtained.

1) Ultra-lean combustion is realized when a backflow of burned gas is formed by the centrifugal force due to rotation, similarly to the methane-air case. Under ultra-lean conditions the reaction zone is formed in the backflow region where apparent local burning velocity is slightly negative, which implies that the flame is not propagating but is supported by diffusion of reactants and heat conduction in a very slow convection field just like a diffusion flame.
2) The flame temperature of RCTF is extremely higher than the adiabatic flame temperature throughout the range of condition we investigated, and the deviation is increased as the condition becomes leaner. The observed largest deviation is more than 670 K. This temperature increase is thought to be caused by so-called low Lewis number effect only inside the ordinary limit of flammability, while in the ultra-lean condition some other effect of increasing temperature works.
3) The composition of the burned gas is quite different from the equilibrium composition. To quantify the difference, we introduced a pseudo local equivalence ratio ϕ_{PL} and it varies largely as a fluid element goes through the flame zone. The ϕ_{PL} in the burned gas amounts to 3.71 times as large as the original equivalence ratio under the leanest condition investigated. This large value of ϕ_{PL} is attributed to the extremely large concentration H_2O in the burned gas, which is presumed to be closely related to the extremely large increase of flame temperature, but its mechanism has not

been clarified.

4) Radiative heat loss has only a small effect on the flame response even under ultra-lean conditions, unlike the methane-air case.

ACKNOWLEDGEMENT

This research was supported by the grant from University of Tsukuba Research Infrastructure Support Program.

REFERENCE

1) D. Dunn-Rankin (Ed.), Lean Combustion – Technology and Control, Academic Press, 2008.
2) M. Nishioka, Z. Shen, A. Uemichi, Combust. Flame 158 (2011) 2188-2198.
3) P.D. Ronney, Combust. Flame 82 (1990) 1-14.
4) J. Buckmaster, G. Joulin, P. Ronney, Combust. Flame 79 (1990), 381-392.
5) Z.H. Chen, G.E. Liu, S.H. Sohrab, Combustion Science and Technology 51 (1987) 39-50.
6) Z. Qin, V.V. Lissianski, H. Yang, W.C. Gardiner, S.G. Davis, H. Wang, Proc. Combust. Inst. 28 (2000) 1663-1669.
7) R.J. Kee, J.F. Grcar, M.D. Smooke, J.A. Miller, Sandia Report, SAND85-8240, 1985.
8) R.J. Kee, F.M. Rupley, J.A. Miller, Sandia Report, SAND89-8009, 1990.
9) B. Lewis, G. von Elbe, Combustion, Flames and Explosions of Gases, 3rd Ed., Academic Press, 1987, 707.
10) B. Lewis, G. von Elbe, Combustion, Flames and Explosions of Gases, 3rd Ed., Academic Press, 1987, 323-333.
11) F. Williams, J. Grcar, Proceedings of the Combustion Institute 32 (2009) 1351-1357.
12) Z.H. Chen and S.H. Sohrab, Combust. Flame 102 (1995) 193-199.
13) C.K. Law, Combustion Physics, Cambridge University Press, 2006, 410-413.
14) Y. Ju, K. Maruta, T. Niioka, Appl. Mech. Rev. 54 (2001) 257-277.
15) R. Barlow, Combust. Flame 127 (2001) 2102-2118.

LIST OF FIGURE CAPTIONS

Fig. 1. Model of rotating counterflow twin premixed flame: (a) small rotation rate case, and (b) large rotation rate case.

Fig. 2. Response of the maximum temperature to the equivalence ratio ϕ: (top) u_R = 400 cm/s with Ω a parameter, and (bottom) Ω = 100rps with u_R a parameter. Dashed lines show adiabatic flame temperatures.

Fig. 3. Maximum temperature T_{max} and burning velocity Su of 1D planer premixed flame as functions of equivalence ratio ϕ.

Fig. 4. Comparison of flame structures at ϕ = 0.15: (left) 1D flame, (right) RCTF at u_R = 400cm/s and Ω = 150 rps.

Fig. 5. Structures of the flame and the flow field for ϕ = 0.20 and u_R = 400 cm/s: temperature, heat release rate and axial velocity u. Vertical lines show the location of the secondary stagnation point x_{stag}. Chain, break, dotted and solid lines shows Ω = 150, 100, 50 and 0 rps, respectively.

Fig. 6. Ultra-lean flame structures for ϕ = 0.08: solid, chain and dotted lines shows Ω = 200, 150 and 100 rps, respectively. Vertical lines show the locations of the secondary stagnation point x_{stag}.

Fig. 7. Flame response to the equivalence ratio ϕ for u_R = 400 cm/s: hatched and open circles are for Ω = 100 and 200 rps, respectively. Dotted, solid and chain lines show the locations of secondary stagnation point x_{stag}, the maximum heat release rate x_{Qmax}, and local burning velocity Su_L, respectively.

Fig. 8. Comparison between chemical enthalpy flux and conductive heat flux in RCTF for u_R = 400 cm/s and Ω = 150 rps: (a) ϕ = 0.50, (b) ϕ = 0.06. For comparison, the distributions of temperature and H_2 mole fraction are shown in the top parts.

Fig. 9. Distributions of pseudo local equivalence ratio ϕ_{PL} for u_R = 400 cm/s, Ω = 100 rps.

Fig. 10. Pseudo local equivalence ratios as functions of ϕ for u_R = 400 cm/s. ϕ_{PL} is normalized by ϕ.

Fig. 11. Response of the maximum flame temperature to the equivalence ratio for Ω = 100rps. Solid lines and dashed lines show the calculation with radiation and without radiation, respectively.

Fig. 12. Flame structure at ϕ = 0.07, u_R = 400 cm/s and Ω = 100 rps. Solid lines and dotted lines show with and without radiative heat loss, respectively.

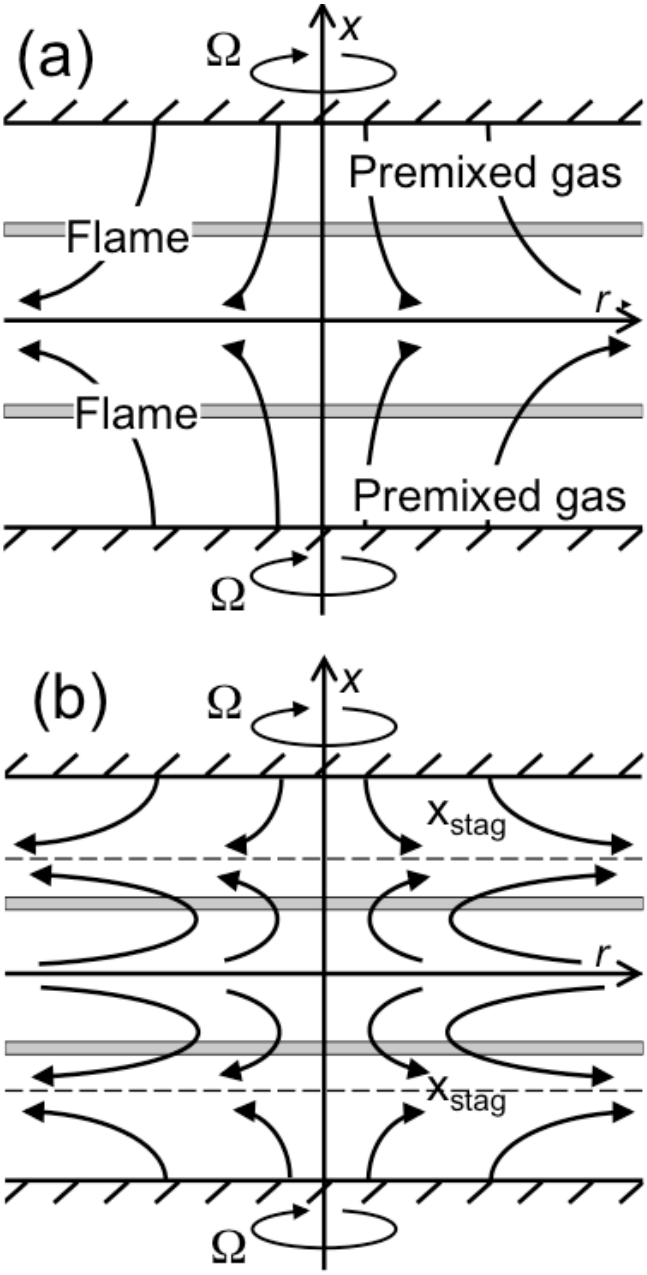

Fig. 1. Model of rotating counterflow twin premixed flame: (a) small rotation rate case, and (b) large rotation rate case.

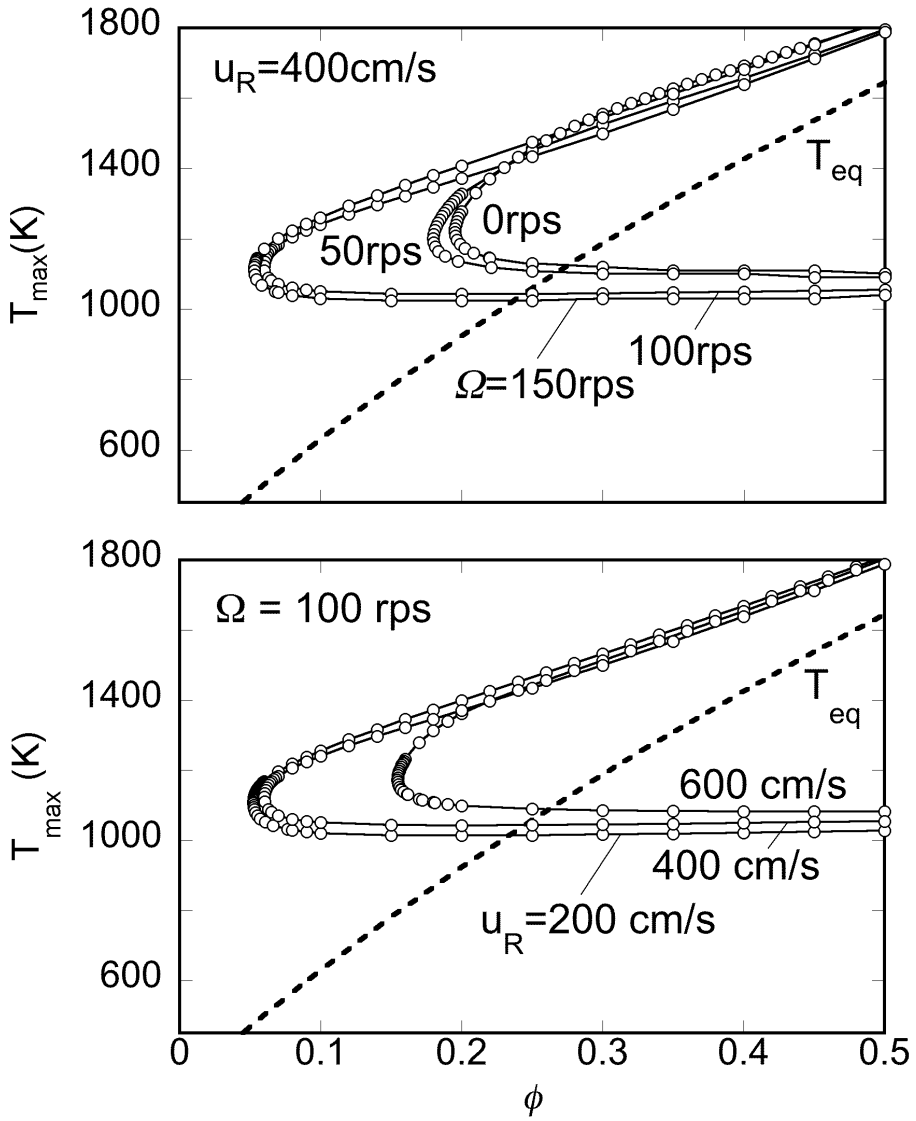

Fig. 2. Response of the maximum temperature to the equivalence ratio ϕ: (top) u_R = 400 cm/s with Ω a parameter, and (bottom) Ω = 100 rps with u_R a parameter. Dashed lines show adiabatic flame temperatures.

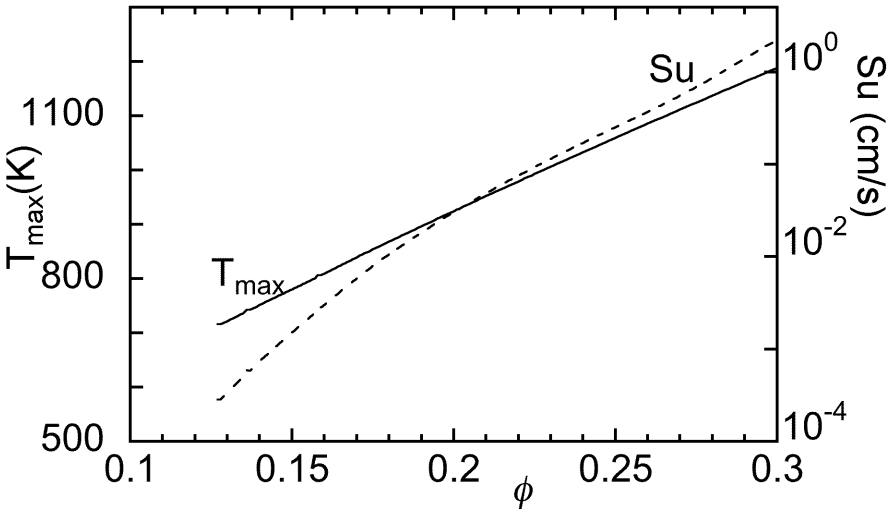

Fig. 3. Maximum temperature T_{max} and burning velocity *Su* of 1D planer premixed flame as functions of equivalence ratio ϕ.

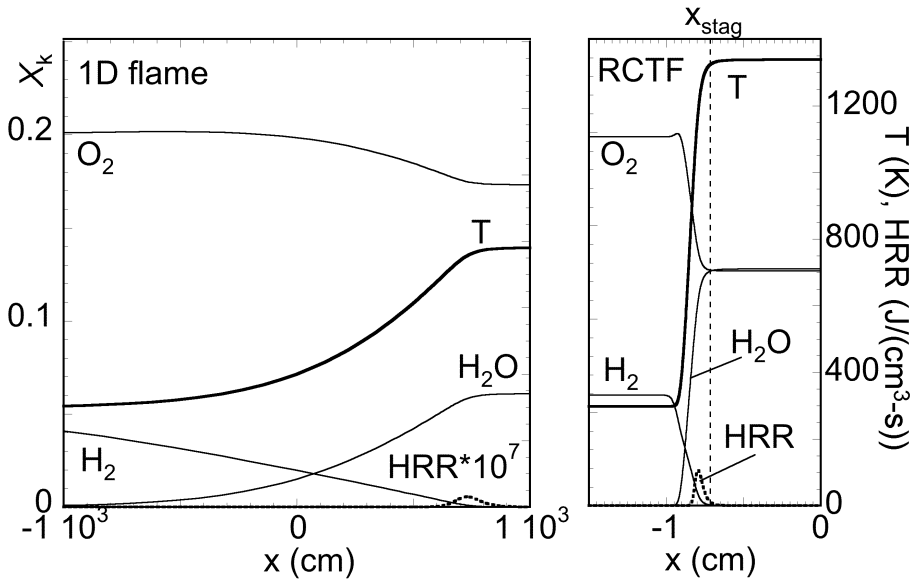

Fig. 4. Comparison of flame structures at $\phi = 0.15$: (left) 1D flame, (right) RCTF at $u_R = 400$ cm/s and $\Omega = 150$ rps.

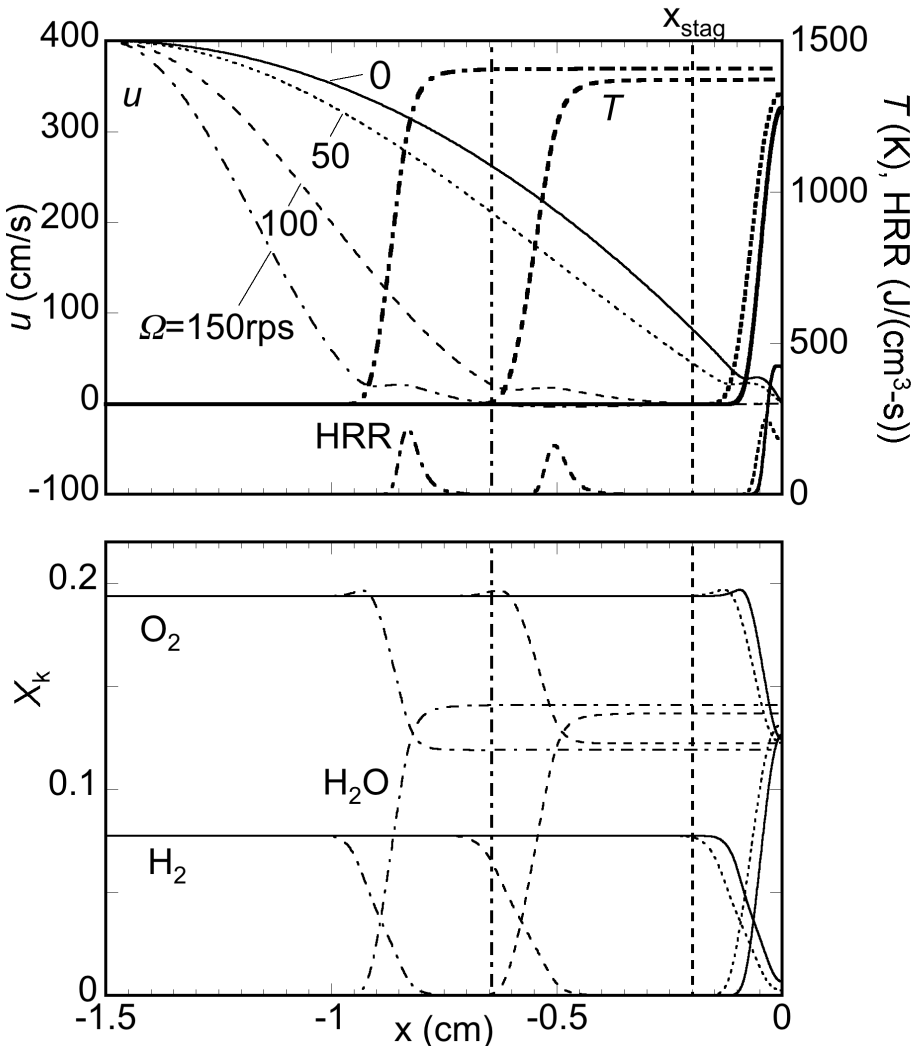

Fig. 5. Structures of the flame and the flow field for $\phi = 0.20$ and $u_R = 400$ cm/s: temperature, heat release rate and axial velocity u. Vertical lines show the location of the secondary stagnation point x_{stag}. Chain, break, dotted and solid lines shows $\Omega = 150$, 100, 50 and 0 rps, respectively.

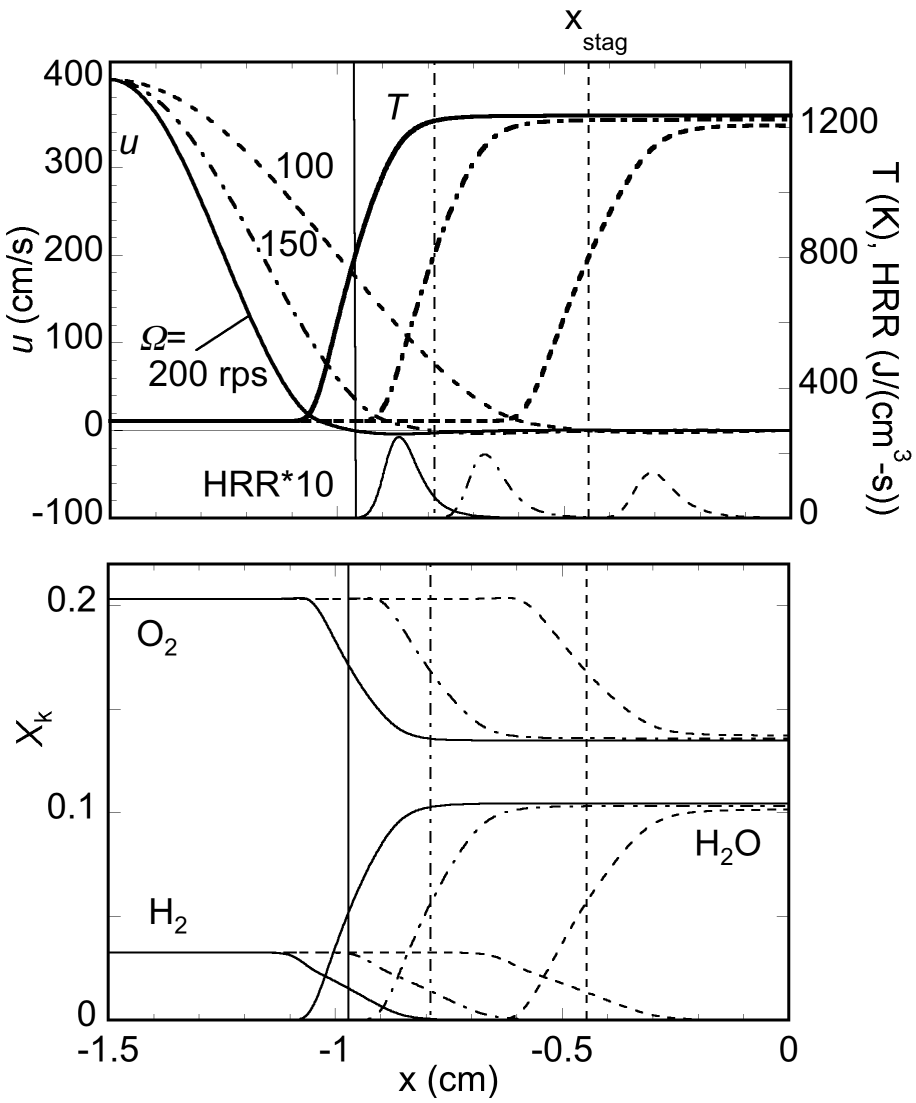

Fig. 6. Ultra-lean flame structures for $\phi = 0.08$: solid, chain and dotted lines shows $\Omega = 200$, 150 and 100 rps, respectively. Vertical lines show the locations of the secondary stagnation point x_{stag}.

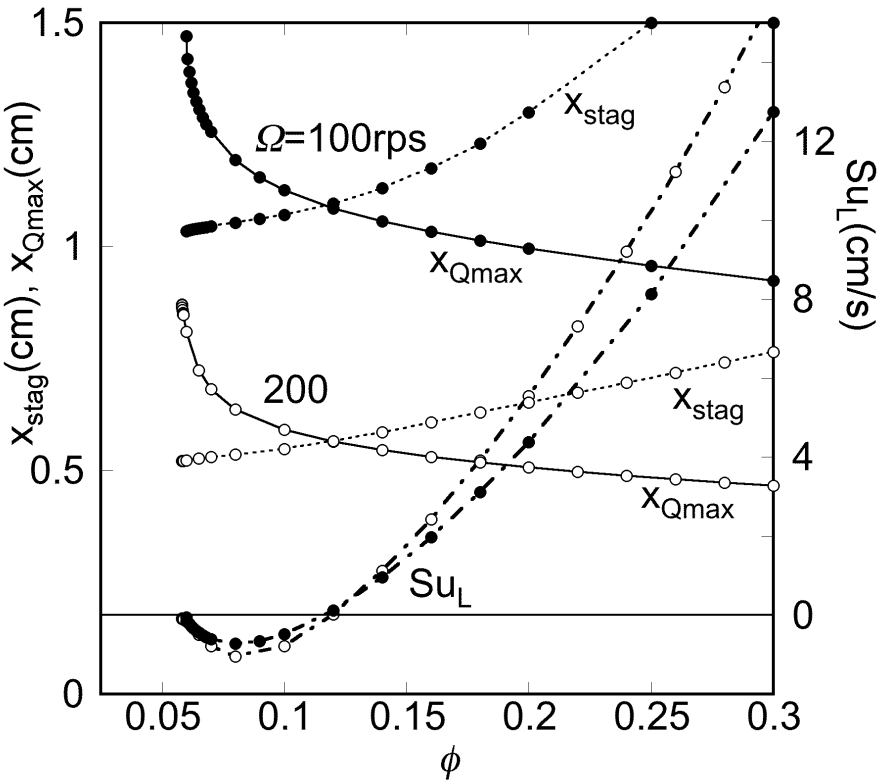

Fig. 7. Flame response to the equivalence ratio ϕ for u_R = 400 cm/s: hatched and open circles are for Ω = 100 and 200 rps, respectively. Dotted, solid and chain lines show the locations of secondary stagnation point x_{stag}, the maximum heat release rate x_{Qmax}, and local burning velocity Su_L, respectively.

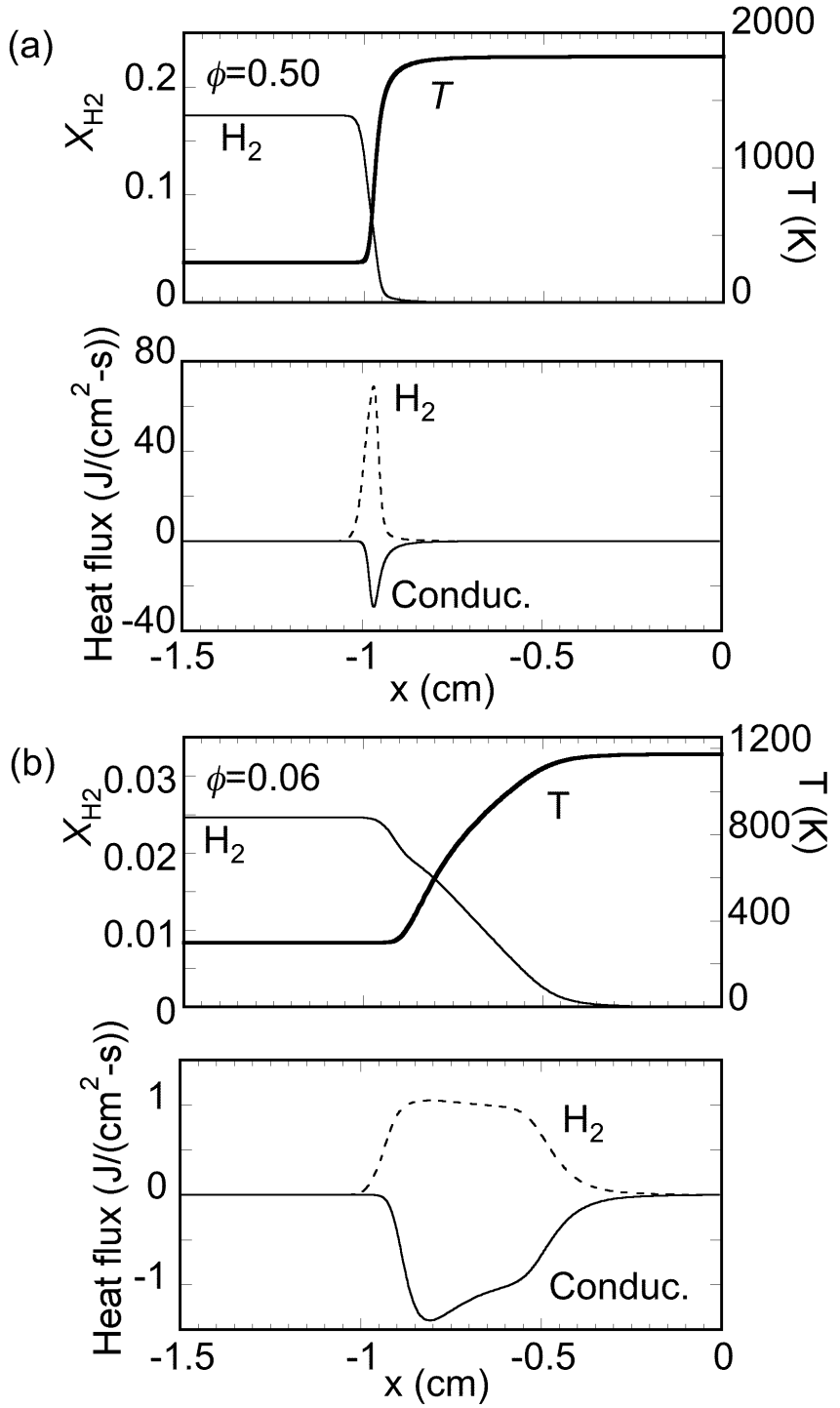

Fig. 8. Comparison between chemical enthalpy flux and conductive heat flux in RCTF for u_R = 400 cm/s and Ω = 150 rps: (a) ϕ = 0.50, (b) ϕ = 0.06. For comparison, the distributions of temperature and H_2 mole fraction are shown in the top parts.

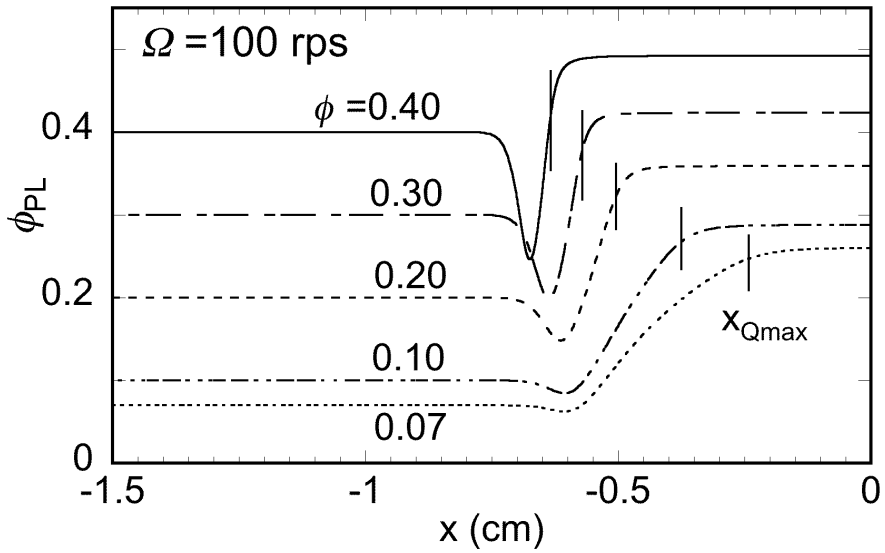

Fig. 9. Distributions of pseudo local equivalence ratio ϕ_{PL} for $u_R = 400$ cm/s, $\Omega = 100$ rps.

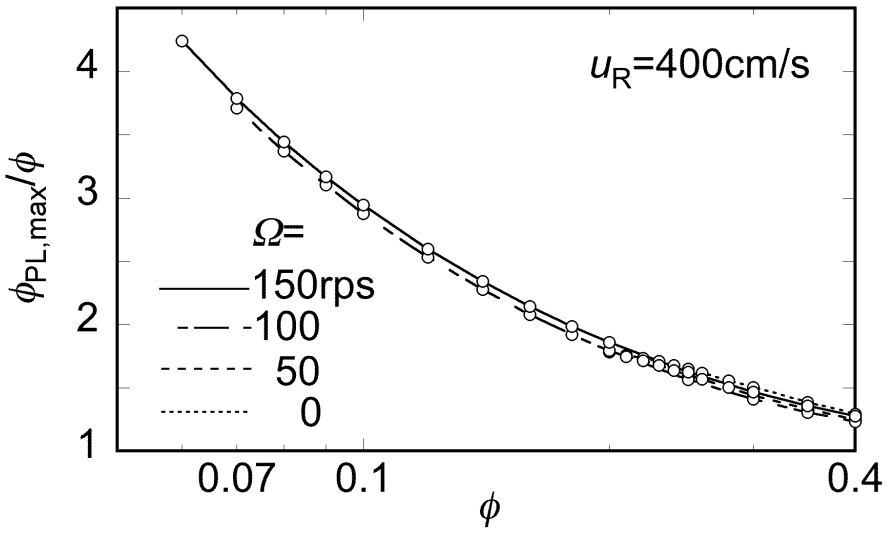

Fig. 10. Pseudo local equivalence ratios as functions of ϕ for u_R = 400 cm/s. ϕ_{PL} is normalized by ϕ.

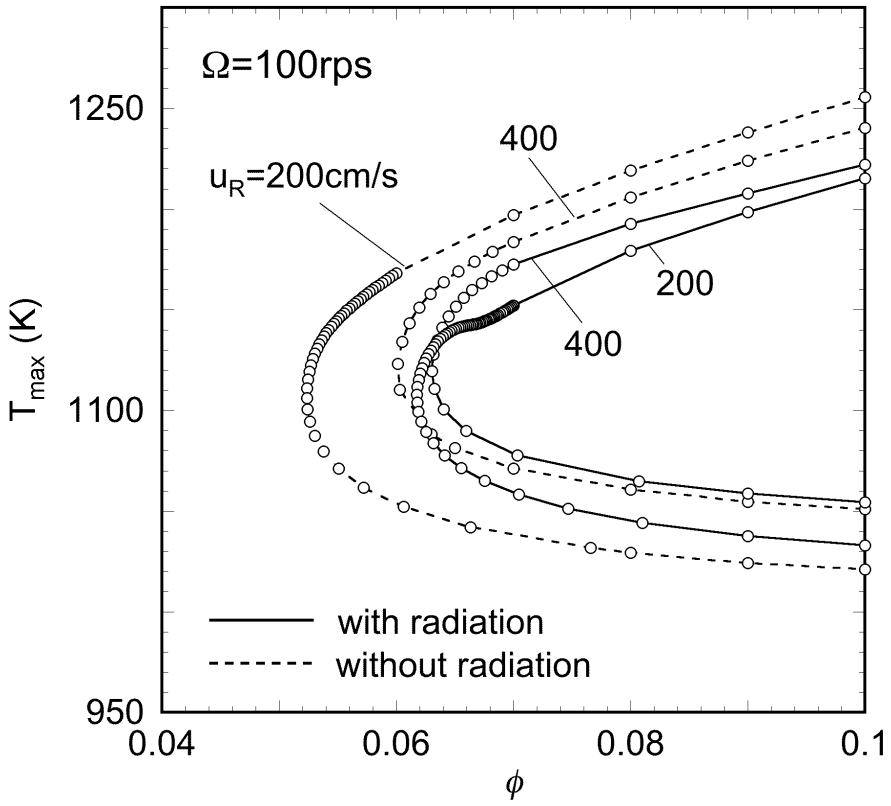

Fig. 11. Response of the maximum flame temperature to the equivalence ratio for Ω = 100 rps. Solid lines and dashed lines show the calculation with radiation and without radiation, respectively.

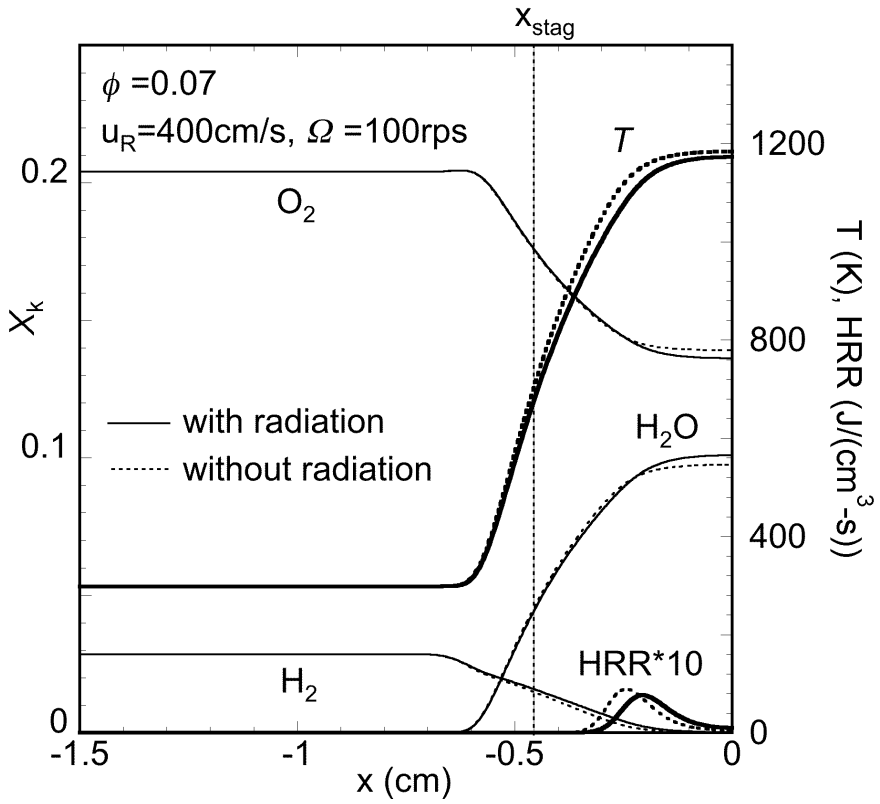

Fig. 12. Flame structure at $\phi = 0.07$, $u_R = 400$ cm/s and $\Omega = 100$ rps. Solid lines and dotted lines show with and without radiative heat loss, respectively.